Conformation and Mobility of 1,4-*trans*-Polybutadiene in the Crystalline State

Yongjian Zhan and Wayne L. Mattice*

Institute of Polymer Science, The University of Akron, Akron, Ohio 44325-3909

Received August 5, 1991; Revised Manuscript Received October 15, 1991

ABSTRACT: Simulations of the molecular dynamics of 1,4-*trans*-polybutadiene in the low- and high-temperature polymorphs (form I and form II, respectively) are compared with the simulation of the polymer as an inclusion complex in the channel of crystalline perhydrotriphenylene. The only internal motions of the dihedral angles in form I on the nanosecond time scale at 300 K are fluctuations of each dihedral angle about its mean value. The fluctuations in form I are smaller than the fluctuations in the other systems. At 360 K form II exhibits strongly correlated rotational isomeric state transitions of the type $A^{\pm}TA^{\mp} \rightarrow A^{\mp}TA^{\pm}$, where A denotes an anticlinal state at a CH–CH_2 bond and T denotes a trans state at a CH=CH or CH_2–CH_2 bond. The CH–CH_2 bond is more mobile in the inclusion complex at 300 K than in form II at 360 K. The cis state is of negligible occurrence in form I, in form II, and in the inclusion complex, but it does occur as an important minor constituent at the CH–CH_2 bonds in the isolated chain.

Introduction

1,4-*trans*-Polybutadiene has two crystalline polymorphs.[1-3] Their structures have been described by Suehiro and Takayanagi.[2] The low-temperature modification, designated as form I, exists at ambient temperature. The conformation of the chain in form I is $A^{\pm}TA^{\mp}T$, with the anticlinal placements (A) occurring at the CH–CH_2 bonds and the trans (T) placements occurring at the CH=CH and CH_2–CH_2 bonds. The chains in form I are packed in a hexagonal array, with the nearest interchain distance a = 4.60 Å and fiber period c = 4.83 Å. Form II exists between approximately 75 and 135 °C. The conformation of the chain in form II is similar to the conformation in form I, except that the dihedral angle for the $A^{\pm}$ states is ±100° from the T state, in contrast to the value of ±71° in form I. Form II is of lower density, and it has a shorter fiber period (c = 4.66 Å).

De Rosa et al. proposed a different disordered conformation for form II, based on calculations of the energy of the packing of the chains.[4] This structure contained an equilibrating equimolar mixture of segments with the conformations $A^{\pm}TA^{\mp}T$ and $CTA^{\pm}T$, where C denotes cis. One-quarter of the CH–CH_2 bonds adopt C states in this mixture.

The details of the conformation and mobility of form II remain the subject of interest.[5] High-resolution solid-state ^{13}C NMR spectroscopy has shown that the chemical shifts and spin–lattice relaxation times of form II are similar to those of the polymer as an inclusion complex in crystalline perhydrotriphenylene.[6] It was suggested that the polymer may undergo similar motions in form II and in the channel formed by crystalline perhydrotriphenylene.[6]

Monomers of several common polymers, including 1,3-butadiene, can diffuse into the channel in crystalline perhydrotriphenylene. Irradiation induces polymerization of the monomers in the channel by a free-radical mechanism. The matrix of perhydrotriphenylene undergoes changes in its lattice during this polymerization. However, neither the polymer nor the monomer is observed directly in the X-ray diffraction pattern obtained after polymerization.[7] Either the polymer is disordered in the channels or the chain undergoes sufficient motion within the channel so that the scattering from it is dynamically averaged.

Solid-state deuterium NMR spectroscopy was used to obtain information on the motions of 1,4-*trans*-poly(butadiene-*1,1,4,4,-d*$_4$) in the channels of crystalline perhydrotriphenylene.[8] The polymer undergoes rapid ($\tau_c \leq 10^{-7}$ s) diffusional motions about the cylindrical axis, thereby producing complete conformational averaging of the C–^{2}H bond vector about this axis during the lifetime of the experiment. Simulation of the molecular dynamics of the polymer in the channel showed that strongly coupled rotational isomeric state transitions at CH–CH_2 bonds i and $i \pm 2$, as represented by

$$A^{\pm}TA^{\mp} \rightleftarrows A^{\mp}TA^{\pm} \quad (1)$$

are fast enough to produce the randomization of the C–^{2}H bond vector that is demanded by the experiment.[9]

Since 1,4-*trans*-polybutadiene undergoes similar motions in the channel of crystalline perhydrotriphenylene and in form II and since there is imperfect knowledge about the conformation, degree of order, and dynamics in form II, we were motivated to study this system by simulations of the molecular dynamics. Here we report the results of the simulations for crystalline 1,4-*trans*-polybutadiene in the solid state and make comparisons with the results of simulations of the molecular dynamics of the polymer in the channel of crystalline perhydrotriphenylene.

Methods

The molecular dynamics trajectories were calculated using version 2.1 of CHARMm,[10] which was supplied by Polygen Corp. The potential energy of the system, E, was calculated as

$$E = E_{\text{stretch}} + E_{\text{bend}} + E_{\text{dihedral}} + E_{\text{improper}} + E_{\text{vdW}} \quad (2)$$

without inclusion of any electrostatic contribution. Four bond angles in the polymer and the form of the intrinsic torsional potential at the CH–CH_2 bond were changed from the values supplied with CHARMm2.1, as described previously.[9] The mobile chain contained ten monomer units and was terminated by methyl groups. All hydrogen atoms were considered explicitly.

The simulations of crystalline 1,4-*trans*-polybutadiene employed seven methyl-terminated chains packed in a hexagonal array. The central mobile chain was surrounded

0024-9297/92/2225-1554$03.00/0

by six immobile chains, each with a degree of polymerization of 15. The system contained 1014 discrete atoms. Each chain was initially constructed so that the conformation was $A^{\pm}TA^{\mp}T$, with the dihedral angles for the $A^{\pm}$ states being ±71° from T for form I and ±100° from T for form II. Unit cells of the sizes proposed by Suehiro and Takayanagi[2] were used. The dimensions were $a = 4.60 \pm 0.01$ Å, $c = 4.83 \pm 0.20$ Å, $\gamma = 120°$ for form I and $a = 4.95 \pm 0.01$ Å, $c = 4.66 \pm 0.20$ Å, $\gamma = 120°$ for form II.

The initial structure of the channel of crystalline perhydrotriphenylene for the simulation was constructed using the information provided by X-ray analysis.[7] The crystalline matrix consists of 90 molecules of perhydrotriphenylene which are arranged in 6 stacks of 15 molecules each.[9] The size of the unit cell is $a = b = 14.26 \pm 0.01$ Å, $c = 4.78 \pm 0.01$ Å, $\gamma = 120°$. The mobile chain of 1,4-*trans*-polybutadiene, initially with all internal bonds in the trans conformation, is located in the channel. In the simulations reported here, the matrix of perhydrotriphenylene was rigid. The system contained 4422 atoms.[9]

The potential energy of each system was first minimized using a conjugate gradient method. The simulation was then initiated with zero kinetic energy, and the temperature was increased in 2 ps, using a time step of 0.2 fs, to either 300 K (for form I and for the polymer as the inclusion complex in perhydrotriphenylene) or 360 K (for form II). After another 2 ps of equilibration, also with a time step of 0.2 fs, the simulation was performed at constant temperature with a time step of 0.5 fs. The lengths of the trajectories are 1 ns. The Z axis of the coordinate system is parallel to the c axis of the crystal.

The $A^{\pm} \rightarrow A^{\mp}$ transitions counted in the present work are a larger set than those that were considered in the simulation reported by Dodge and Mattice.[9] That study focused on transitions in which a $CH-CH_2$ bond "rotated from $A^{\pm}$ to $A^{\mp}$ and remained in the new state for at least 5 ps". Here we consider all transitions at the $CH-CH_2$ bonds, including those transitions in which the new state has a lifetime less than 5 ps. This distinction is important because there are many transitions at the $CH-CH_2$ bonds that produce new states with very short lifetimes. (The average lifetimes in the inclusion complex are only about 1 ps for the internal $CH-CH_2$ bonds in the sequences $A^{\pm}TA^{\pm}TA^{\pm}$ and $A^{\pm}TA^{\pm}TA^{\mp}$.)

Results and Discussion

Distribution Functions for the Dihedral Angles. The dihedral angles at the C–C bonds in the internal six monomer units of the mobile chain were monitored during the simulations. The distribution functions for the dihedral angles at the $CH-CH_2$ bonds are depicted in Figure 1. The dihedral angle is depicted as the absolute value of $\phi - \phi_T$, where ϕ_T denotes the dihedral angle for a T placement. The three distribution functions have in common the appearance of maxima in the region expected for $A^{\pm}$ placements and negligible probability in the region of the C placement. They differ in the precise locations of the maxima, in the widths of the peaks, and in the extension of the wings of the distribution to the vicinity of a T placement.

Quantitative comparison is facilitated by evaluation of $\langle|\phi - \phi_T|\rangle$ and $\delta|\phi - \phi_T|$, where the angle brackets denote the average of the enclosed quantity and

$$\delta|\phi - \phi_T| = (\langle|\phi - \phi_T|^2\rangle - \langle|\phi - \phi_T|\rangle^2)^{1/2} \quad (3)$$

These quantities are presented in Table I, along with the results obtained from an isolated chain of 1,4-*trans*-polybutadiene at 300 K. The values of $\langle|\phi - \phi_T|\rangle$ at the $CH-CH_2$ bonds fall within a range of 14°, with the extremes being provided by form II and the inclusion complex in perhydrotriphenylene. These differences in $\langle|\phi - \phi_T|\rangle$ for the extremes arise predominantly from the differences in the shapes of the distribution functions, because the values of $|\phi - \phi_T|$ at the maxima lie within an interval of only 2° for form II and the inclusion complex. The distribution function for the inclusion complex has a more pronounced wing at very small values of $|\phi - \phi_T|$, causing it to have a small value of $\langle|\phi - \phi_T|\rangle$. Form I has the narrowest distribution function, as shown by the small value of $\delta|\phi - \phi_T|$.

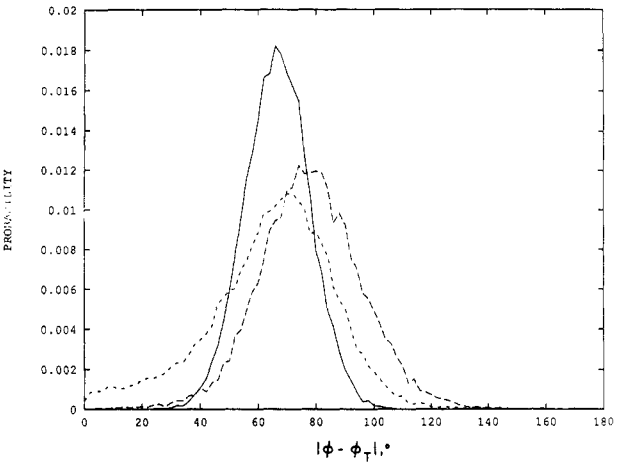

Figure 1. Distribution function at 300 K for the dihedral angles at the $CH-CH_2$ bonds in the internal six monomer units in the mobile chain in form I (solid line), form II (line with long dashes), and the inclusion complex (line with short dashes). The dihedral angle for a trans placement is denoted by ϕ_T.

Table I
$\langle|\phi - \phi_T|\rangle$ and $\delta|\phi - \phi_T|$ (deg)

bond	system	$\langle\lvert\phi - \phi_T\rvert\rangle$	$\delta\lvert\phi - \phi_T\rvert$
$CH-CH_2$	form I	66	11
	form II	78	18
	PHTP-IC[a]	64	22
	isolated chain	68	29
CH_2-CH_2	form I	5	3
	form II	8	7
	PHTP-IC	6	5
	isolated chain	68	56
CH=CH	form I	5	4
	form II	8	7
	PHTP-IC	7	6
	isolated chain	8	6

[a] Inclusion complex in crystalline perhydrotriphenylene.

The large value of $\delta|\phi - \phi_T|$ for the isolated chain arises because it sometimes has a C placement at the $CH-CH_2$ bond. The maximum probability in the region of the C placement is about 6% of the maximum probability in the region of the $A^{\pm}$ placements in the isolated chain. In contrast, the probability is nil in the region of the C placement for form I, form II, and the inclusion complex, as shown in Figure 1. The results presented in Figure 1 do not support the suggestion[8] that $CTA^{\pm}T$ sequences occur to the extent of 25% in form II and in the inclusion complex. The C states at the $CH-CH_2$ bonds are of very rare occurrence in the simulations of these two systems. They produce a conformation that does not fit as easily in a narrow channel as the one with $A^{\pm}$ placements, as shown in Figure 7 of ref 9.

One argument presented in favor of the presence of C placements at the $CH-CH_2$ bonds in form II and in the inclusion complex in perhydrotriphenylene is the fact that the chemical shifts in the ^{13}C NMR spectra for the polymer

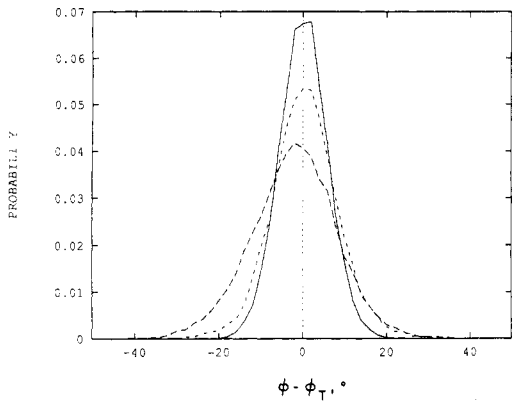

Figure 2. Distribution function at 300 K for the dihedral angles at the CH_2–CH_2 bonds in the internal six monomer units in the mobile chain in form I (solid line), form II (line with long dashes), and the inclusion complex (line with short dashes).

in these two systems are different from those observed in form I.[5,6] The difference was rationalized using the anticipated γ-gauche shielding interactions for the A and C states. The difference in the ^{13}C NMR spectra would be hard to reconcile with the present simulations if attention was confined to $\langle|\phi - \phi_T|\rangle$ for the CH–CH_2 bond. As shown in Table I, nearly identical averages are observed for form I, the inclusion complex, and the isolated chain, and a value $12 \pm 2°$ larger is obtained for form II. However, inspection of Figure 1 causes one to wonder whether the averages might be misleading. Form II and the inclusion complex are distinguishable from form I more by virtue of the breadth of the distribution than by the value of $\langle|\phi - \phi_T|\rangle$. A quantitative measure of the breadth is $\delta|\phi - \phi_T|$. As shown by the last column in Table I, similar values of $\delta|\phi - \phi_T|$ are obtained for form II and the inclusion complex, and the values are nearly twice as large as $\delta|\phi - \phi_T|$ for form I. The breadth of the distribution in the wing where ϕ approaches ϕ_T is responsible for the ease of $A^+ \rightarrow A^-$ transitions in the inclusion complex and in form II, in contrast with the absence of these transitions in form I. Quantitative evaluation of the influence of the difference in the shapes of the distribution functions would require an accurate expression for the γ-gauche shielding interaction as a continuous function of ϕ over the entire range.

The values of ϕ at the CH_2–CH_2 bonds are restricted to the region of the T placement in form I, form II, and the inclusion complex, as shown in Figure 2 and by the small values of $\langle|\phi - \phi_T|\rangle$ and $\delta|\phi - \phi_T|$ in Table I. The distribution is slightly narrower for form I than for form II or the inclusion complex. Slight departure from the anticipated symmetry in Figure 2 can be attributed to the finite length of the trajectories. There is no evidence whatsoever for the occupation of gauche states by the mobile chain in form I, form II, or the inclusion complex, but these states are strongly populated during the simulation of the isolated chain, leading to large values of $\langle|\phi - \phi_T|\rangle$ and $\delta|\phi - \phi_T|$ for the last entry for CH_2–CH_2 in Table I. The confinement of the distribution of dihedral angles at the CH_2–CH_2 bonds in form I, form II, and the inclusion complex is comparable with that seen at the CH=CH bonds, as shown in Table I.

The entries in Table I show that every type of bond has a larger value of $\delta|\phi - \phi_T|$ in form II than in form I. This observation in the simulations is consistent with the description of form II as being a more disordered crystal than form I.[2,5] Coordinated transitions at bonds i and $i \pm 2$, to be presented below, are an additional source of disorder in form II.

Table II
Average Lifetimes (ps) for Anticlinal States at the Internal CH–CH_2 Bonds in Three Sequences

sequence	form II, 360 K	inclusion complex, 300 K
$A^{\pm}TA^{\pm}TA^{\pm}$	1	1
$A^{\pm}TA^{\mp}TA^{\mp}$	46	1
$A^{\pm}TA^{\mp}TA^{\pm}$	108	6

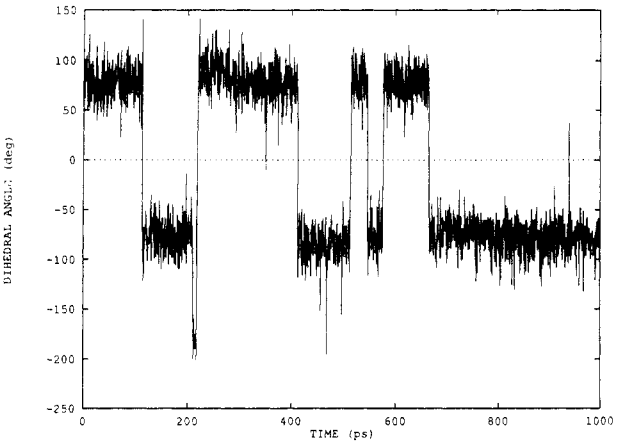

Figure 3. History of the dihedral angle at a CH_2–CH bond (bond i) in form II at 360 K.

Transitions between Rotational Isomeric States. Figure 1 shows the occupation of two rotational isomeric states, denoted $A^{\pm}$, at the CH–CH_2 bonds. The differences in the sizes of the wings of the distribution functions at $\phi = \phi_T$ suggest that there will be differences in the rates of the interconversions between these two rotational isomeric states.

No rotational isomeric state transitions were observed at the CH–CH_2 bonds in form I during a trajectory of 1-ns duration. Instead there were rapid fluctuations of the dihedral angles about their most probable values, with the magnitudes of these fluctuations being depicted in Figure 1 and quantified by $\delta|\phi - \phi_T|$ in Table I.

The mobility of the CH–CH_2 bonds in form II and in the inclusion complex depends on the state of the two next-nearest-neighbor CH–CH_2 bonds. There is an increase in mobility if either or both next-nearest neighbors occupy an anticlinal state of the same sign, as shown in Table II. The middle bond in the sequence $A^{\pm}TA^{\pm}TA^{\pm}$ has an average lifetime of only $\approx$1 ps in form II and in the inclusion complex. A lifetime nearly 2 orders of magnitude longer is seen for the middle bond in the sequence $A^{\pm}TA^{\mp}TA^{\pm}$ in form II. The lifetimes in Table II show that the chain in the inclusion complex has greater internal mobility than the chain in form II.

Coupled rotational isomeric state transitions, as represented by eq 1, are observed at bonds i and $i \pm 2$ in form II. These transitions are accompanied by large changes in the orientation of the C–H bond vectors attached at either end of the internal bond that remains in the T state while its neighbors undergo the correlated transitions. There are two such C–H bond vectors when the internal bond is CH=CH and four such bond vectors if it is CH_2–CH_2. Figures 3 and 4 depict two correlated transitions for the case where the internal bond, $i + 1$, is CH=CH. The history of the dihedral angles at bonds i and $i + 2$ is presented in Figures 3 and 4, respectively. There are correlated rotational isomeric state transitions, according to eq 1, at 113 and 217 ps. The second transition is preceded by a very brief excursion, of about 8-ps duration, by bond i to the C state. This excursion is correlated with a transition at bond $i - 2$. Bond i also has five rotational

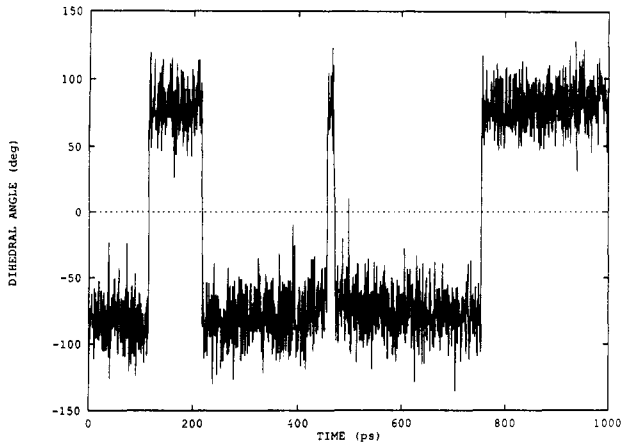

Figure 4. History of the dihedral angle at a CH–CH_2 bond (bond $i + 2$) in form II at 360 K.

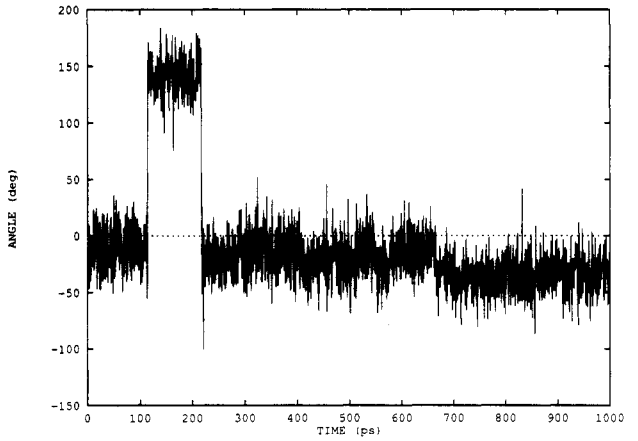

Figure 5. History of the orientation of the projection onto the XY plane of the C–H bond vector to the italicized hydrogen atom in CH_2–C*H*=CH–CH_2. The C–C bonds are i, $i + 1$, and $i + 2$ of Figures 3 and 4.

isomeric state transitions at $t > 400$ ps that have no counterpart at bond $i + 2$. These transitions at bond i are paired instead with transitions at bond $i - 2$. In general, the coordinated rotational isomeric state transitions typically cause the dihedral angles at the CH–CH_2 bonds to stay in their new $A^{\pm}$ states for more than 5 ps, as illustrated by the paired transitions depicted in Figures 3 and 4. When averaged over the internal six monomer units, each triplet of bonds centered on CH=CH or CH_2–CH_2 experiences an average of four $A^{\pm}TA^{\mp} \rightarrow A^{\mp}TA^{\pm}$ transitions every nanosecond.

Figures 5–7 depict the motion of selected C–H bond vectors in the segment that is affected by the rotational isomeric state transitions presented in Figures 3 and 4. The angle plotted in Figures 5–7 is between the X axis and the projection of the C–H bond vector onto the XY plane. Consequently, this angle shows the orientation of a selected bond from the polymer in an external coordinate system defined by the rigid matrix, whereas the dihedral angles used in Figures 3 and 4 are defined by an internal coordinate system based on two consecutive bonds in the polymer. Figures 5 and 6 show the orientations of the C–H bond vectors at either end of the CH=CH bond, bond $i + 1$, that lies between the coupled transitions at 113 and 217 ps. These two C–H bond vectors always tend to point in opposite directions, due to the occupancy of the T state at the double bond. They trade directions when the CH_2–CH bonds on either side execute the paired rotational isomeric state transitions according to eq 1. These two C–H bond vectors are unaffected by the

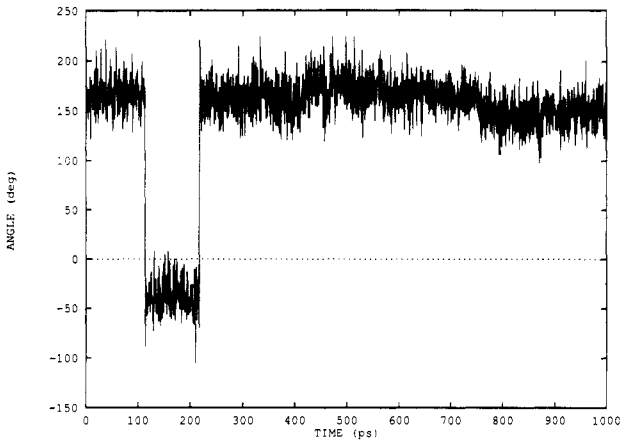

Figure 6. History of the orientation of the projection onto the XY plane of the C–H bond vector to the italicized hydrogen atom in CH_2–CH=C*H*–CH_2. The C–C bonds are i, $i + 1$, and $i + 2$ of Figures 3 and 4.

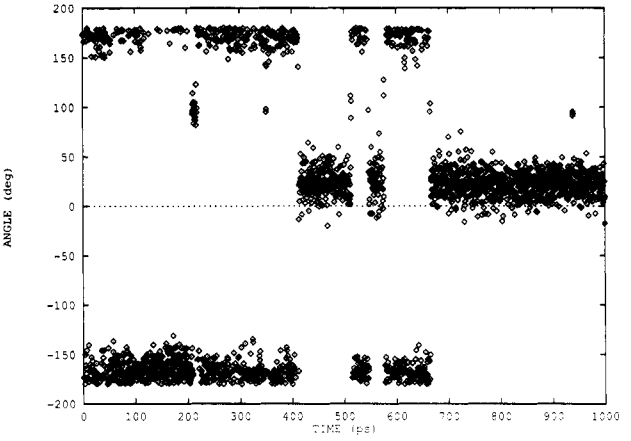

Figure 7. History of the orientation of the projection onto the XY plane of the C–H bond vector to the italicized hydrogen atom in CH*H*–CH=CH–CH_2. The C–C bonds are i, $i + 1$, and $i + 2$ of Figures 3 and 4.

additional rotational isomeric state transitions that occur at 209 and at $t > 400$ ps in Figure 3. It is the orientation of the C–H bond vectors in the methylene group at the other end of this CH_2–CH bond, bond i, that is affected, as shown in Figure 7.

Figures 5 and 6 show that there is negligible rotation of the entire chain about its long axis during the simulation. The angle does not move in a systematic manner in the absence of an internal conformational change, as demonstrated by similar values for the averages of the angles during the first and last 100 ps of the simulation.

The two different orientations of the C–H bond vectors in Figures 5 and 6 imply the existence of disorder in form II. The consequences are captured in the snapshots depicted in Figure 8. The upper panel of this figure is a snapshot of the mobile chain in form I at the end of the simulation. The left-hand methine group of every CH=CH has the hydrogen atom directed toward the viewer, and the right-hand methine group has its hydrogen atom directed so that it is hidden from view. A different situation is encountered in the bottom panel, which depicts the final conformation of the mobile chain in form II. Reading from left to right along the chain, the first CH=CH unit is normal to the plane of the paper, the next five CH=CH units are oriented such that the right-hand methine group has its hydrogen atom directed toward the viewer, and in the last four CH=CH units it is the left-hand methine group that is so directed. This behavior is

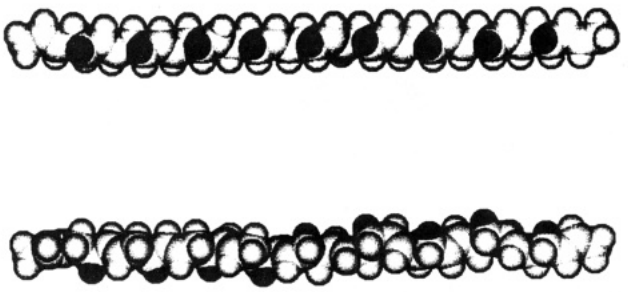

Figure 8. Snapshots of the mobile chain in form I (top) and in form II (bottom) at the end of the simulations. The equivalent hydrogen atom in a CH_2 unit is darkened in each monomer unit.

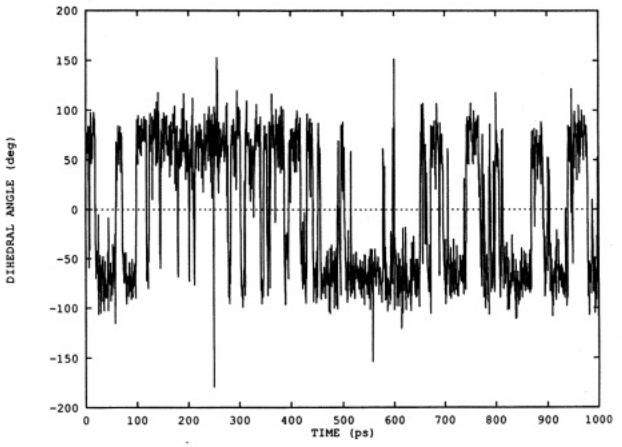

Figure 9. History of the dihedral angle at a CH_2–CH bond in a central monomer unit of the chain in the inclusion complex at 300 K.

reminiscent of the suggestion by Möller that the high mobility of the polymer in form II arises from conformational interconversions in which the chain appears to be broken up into relatively short segments which can undergo independent diffusive rotational motions.[11]

Figure 9 depicts the history of the dihedral angle at a CH–CH_2 bond in one of the central monomer units for the mobile chain in the inclusion complex. Transitions between the $A^{\pm}$ states occur at a greater frequency here than they did in form II (compare with Figures 3 and 4). Some of the transitions in Figure 9, such as those at 56, 70, and 97 ps, are from a state with a lifetime greater than 10 ps to another state that will also have a lifetime greater than 10 ps. These transitions have a high probability of being correlated with a counterrotation at bond $i \pm 2$, as was the case for the transitions in form II. Others of the transitions in Figure 9, such as the closely spaced pairs near 143, 179, and 200 ps, represent very brief (but large) fluctuations away from one of the $A^{\pm}$ states. These brief, but large, fluctuations are usually not correlated with a counterfluctuation at bond $i \pm 2$. These transitory changes were observed previously, and they were defined as fluctuations (as distinct from rotational isomeric state transitions) because they did not involve initial and final states that were stable for at least 5 ps.[9] The true rotational isomeric state transitions between states that are stable for at least 5 ps and that are strongly correlated with transitions at bonds $i \pm 2$ were observed previously in the simulation of a system with a mobile matrix of perhydrotriphenylene.[9] The transitions across the line $\phi = \phi_T$ are more frequent for the chain in the inclusion complex than in form II, as expected from the appearance of the distribution functions depicted in Figure 1.

Motions along the *Z* Axis. Several other types of motions were monitored for the mobile chain. On the nanosecond time scale, all of these motions are best described as fluctuations about a mean value. The magnitudes of the fluctuations are reported here as δZ, defined as $(\langle Z^2 \rangle - \langle Z \rangle^2)^{1/2}$, and δY and δX, which are defined similarly. The values of δX, δY, and δZ are collected in Table III. For each structure, fluctuations of a few tenths of an angstrom are seen along all three axes for each type of carbon atom. The terminal methyl groups exhibit larger fluctuations than the carbon atoms in the interior of the chain in form I and in form II, but in the inclusion complex the ends and interior of the chain experience comparable fluctuations. In comparing carbon atoms at equivalent positions in the chains in all three systems, the smallest fluctuations are found in form I.

Table III
Fluctuations (Å) of the Carbon Atoms

atom	system	δX	δY	δZ
C(H)[b]	form I	0.14	0.14	0.11
	form II	0.28	0.33	0.26
	PHTP-IC[a]	0.39	0.38	0.21
$C(H_2)$[b]	form I	0.15	0.12	0.12
	form II	0.32	0.45	0.26
	PHTP-IC	0.46	0.44	0.22
$C(H_3)$[c]	form I	0.23	0.27	0.19
	form II	0.41	0.46	0.36
	PHTP-IC	0.36	0.37	0.27

[a] Inclusion complex in crystalline perhydrotriphenylene. [b] Average for internal four monomer units. [c] Average for terminal methyl groups.

The fluctuation in the projection of the end-to-end vector onto the *Z* axis defined by the rigid matrix ranges from 0.25 Å in form I to 0.45 Å in form II, which are 0.5–1.0% of the mean value of the end-to-end distance. The time scale for significant translational diffusion through the channel is much longer than the time scale for rotational isomeric state transitions between $A^{\pm}$ states at the CH–CH_2 bonds.

Randomization of C–H Bond Vectors in a Coordinate System Defined by the Channel. We now consider the extent of the randomization of the C–H bond vectors on the nanosecond time scale, using a polar coordinate system defined by the channel. The *Z* axis is parallel to this channel. Let θ denote the instantaneous value of the angle between a chosen C–H bond vector and the *Z* axis. Thus $\theta = 0°$, 90°, and 180° if the C–H vector is parallel, perpendicular, or antiparallel to the *Z* axis. Let ψ denote the instantaneous value of the rotation about the *Z* axis. The values of θ and ψ were recorded at intervals of 0.5 ps, over the trajectory of 1 ns.

Figure 10 depicts the record for a particular C–H bond vector in a –CH= unit in the chain in form II. The values of θ are denoted by the radial distance from the center of the figure, using the numerical scale (in degrees) printed on the two axes. Nearly all of the 2000 snapshots have $40° < \theta < 110°$. The values of ψ are represented by the angle P–O–X, where P is the location of a point on the figure, O denotes the center of the figure, and X denotes the right end of the horizontal dashed line through the middle of the figure. The values of ψ in Figure 10 are taken from Figure 7. They prefer two relatively broad ranges, $-20° < \psi < +60°$ and $-135° > \psi$ or $\psi > +145°$. Transitions between these two broad ranges occur via $\psi = +90°$, instead of via $\psi = -90°$. Not all of the C–H bond vectors in the –CH= units in the chain in form II experience such transitions in 1 ns, as shown by the data for a different –CH= bond vector in Figure 11.

The –CH= bond vectors are much more mobile when the chain is in the inclusion complex. The behavior of a

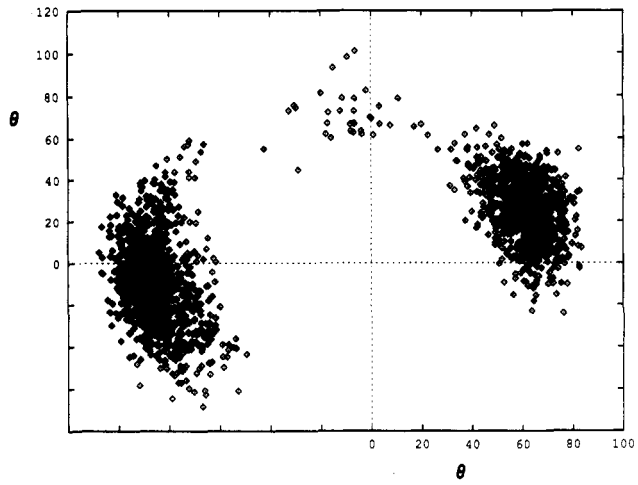

Figure 10. Record of 2000 instantaneous values of θ and ψ, at intervals of 0.5 ps, for a C–H bond vector in a –CH= unit in the chain in form II at 360 K. The value of θ, in degrees, is given by the distance of a point from the intersection of the two dashed lines, using the scale on either axis. The value of ψ is given by the direction of the point from the intersection of the dashed lines.

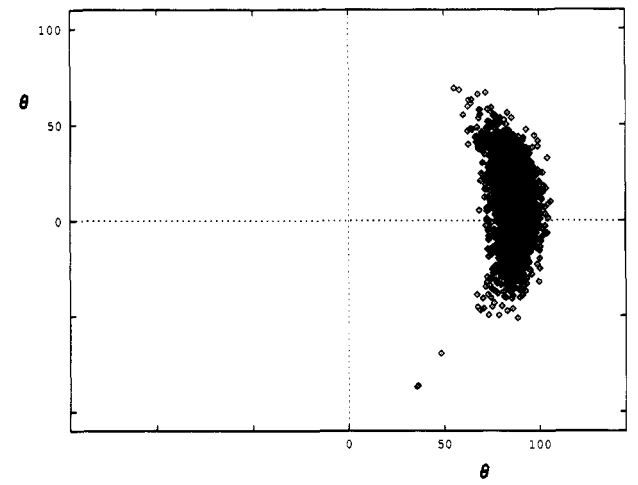

Figure 11. Behavior of θ and ψ over 1 ns for a C–H bond vector in a –CH= unit in form II that has no $A^{\pm} \rightarrow A^{\mp}$ transitions in the CH_2–CH bond nearby.

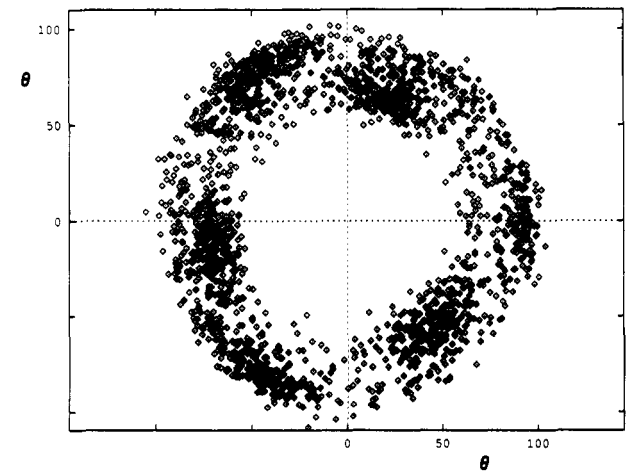

Figure 12. Behavior of θ and ψ over 1 ns for a C–H bond vector in a –CH= unit in the chain in the inclusion complex at 300 K.

representative bond vector is depicted in Figure 12. Randomization of ψ is nearly complete in 1 ns.

Figure 13 depicts equivalent information for a representative C–H bond vector in a CH_2 unit in the chain in

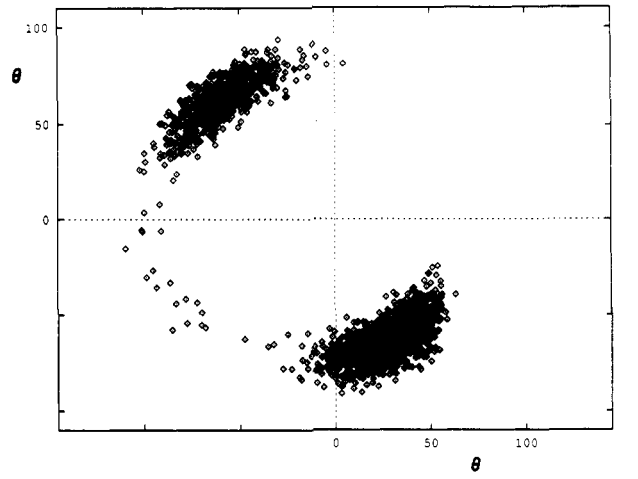

Figure 13. Values of θ and ψ over 1 ns for a C–H bond vector in a CH_2 unit in form II at 360 K.

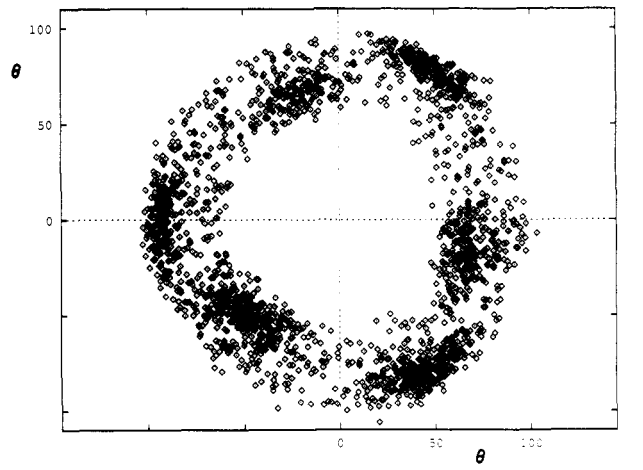

Figure 14. Values of θ and ψ over 1 ns for a C–H bond vector in a CH_2 unit in the chain in the inclusion complex at 300 K.

form II. This vector spends most of the 1-ns trajectory in two broad ranges of ψ, and the transition between the two ranges occurs via $\psi = 90°$. Thus the qualitative behavior is similar to that seen with the –CH= bond vector in Figure 10.

The behavior of a representative C–H bond vector in a CH_2 unit in the chain in the inclusion complex is depicted in Figure 14. Randomization of ψ is nearly complete in 1 ns. The pronounced randomization arises from the broad fluctuations in the internal dihedral angle ϕ (depicted in Figure 1), the transitions between A^+ and A^- states at the CH–CH_2 bond, and the fact that the value of ψ for a particular C–H bond vector can be affected by $A^+ \rightarrow A^-$ transitions in nearby monomer units (i.e., a rotational isomeric state transition at bond i perturbs the value of ψ for C–H bond vectors nearby).

The ten panels in Figure 15 present the data from the 1-ns trajectory (Figure 14) in ten successive portions, each of duration 0.1 ns. Thus each panel in Figure 15 contains 200 of the 2000 points from Figure 14. Several of the 0.1-ns time segments show a strong preference for one quadrant and a strong avoidance of another quadrant (e.g., Figures 15a,b,f,g) and other 0.1-ns time segments show significant population in all four quadrants (e.g., Figures 15e,h).

The distribution for ψ in these panels is responding not only to $A^{\pm} \rightarrow A^{\mp}$ isomerization at the CH–CH_2 bond next to the C–H bond vector. It is also affected by the fluctuations in ϕ within a particular anticlinal state at the

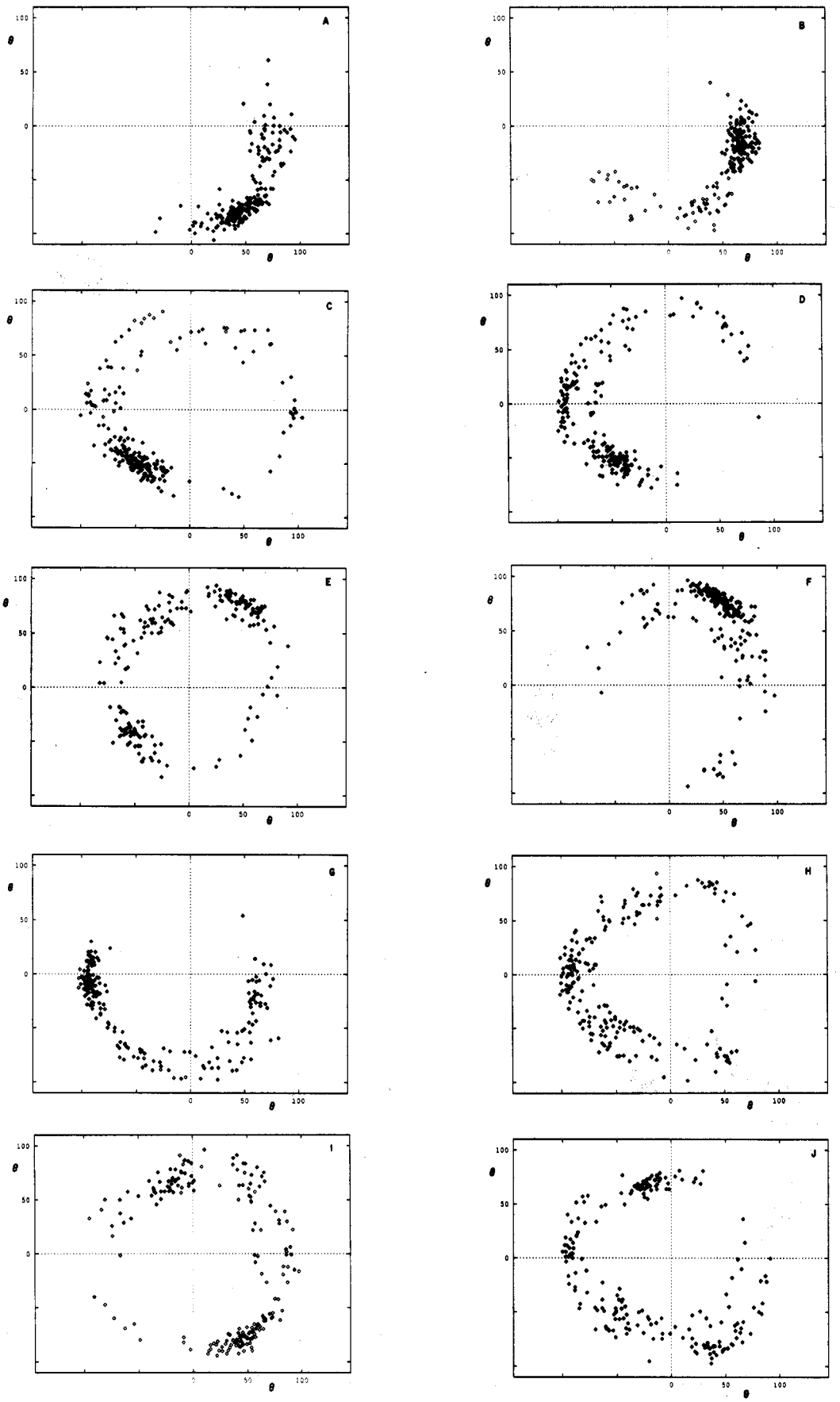

Figure 15. Panels A–J depict points from Figure 14 for ten consecutive time segments of 0.1 ns each.

neighboring $CH–CH_2$ bond (the range of these fluctuations was depicted in Figure 1) and by the cumulative effect of the fluctuations in ϕ at several $CH–CH_2$ bonds on either side. (If n consecutive $CH–CH_2$ bonds were to simultaneously experience a fluctuation in ϕ of size $\Delta\phi$, in the same direction, the cumulative twist through that segment of $2n-1$ bonds is $n\Delta\phi$.) Thus the interplay of the relatively broad fluctuations in ϕ in the anticlinal states contributes

to the rapid randomization of the distribution for ψ.

Conclusions

The principal motions on the nanosecond time scale in form I at 300 K are fluctuations about the mean values of the dihedral angles at the C–C bonds. These fluctuations are smaller in size than the corresponding fluctuations in form II at 360 K or in the inclusion complex at 300 K. The principal motions on the nanosecond time scale in form II at 360 K are strongly correlated transitions of the type $A^{\pm}TA^{\mp} \rightarrow A^{\mp}TA^{\pm}$. These correlated transitions also occur in the inclusion complex at 300 K. In addition, the inclusion complex has frequent large fluctuations at the $CH–CH_2$ bond that correspond to $A^{\pm} \rightleftarrows A^{\mp}$ in which one of the states has a lifetime substantially shorter than 5 ps. The C state is of negligible occurrence in form I, form II, and the inclusion complex, but it does occur in the isolated chain.

Acknowledgment. This work was supported by research grant DMR 89-15025 from the National Science Foundation.

References and Notes

(1) Corradini, P. *J. Polym. Sci., Polym. Lett. Ed.* **1969**, *7*, 211.
(2) Suehiro, J.; Takayanagi, M. *J. Macromol. Sci., Phys.* **1970**, *B4*, 39.
(3) Corradini, P. *J. Polym. Sci., Polym. Symp.* **1975**, *50*, 327.
(4) De Rosa, C.; Napolitano, R.; Pirozzi, B. *Polymer* **1985**, *26*, 2039.
(5) Schilling, G. C.; Gomez, M. A.; Tonelli, A. E.; Bovey, F. A.; Woodward, A. E. *Macromolecules* **1987**, *20*, 2954.
(6) Sozzani, P.; Bovey, F. A.; Schilling, F. C. *Macromolecules* **1989**, *22*, 4225.
(7) Columbo, A.; Allegra, G. *Macromolecules* **1971**, *4*, 579.
(8) Sozzani, P.; Behling, R. W.; Schilling, F. C.; Bruckner, S.; Helfand, E.; Bovey, F. A.; Jelinski, L. W. *Macromolecules* **1989**, *22*, 3318.
(9) Dodge, R.; Mattice, W. L. *Macromolecules* **1991**, *24*, 2709.
(10) Brooks, B. R.; Bruccoleri, R. E.; Olafson, B. D.; States, D. J.; Swaminathan, S.; Karplus, M. *J. Comput. Chem.* **1983**, *4*, 187.
(11) Möller, M. *Makromol. Chem., Rapid Commun.* **1988**, *9*, 107.

Registry No. $H_2C{=}CHCH{=}CH_2$ (homopolymer), 9003-17-2; triphenylene·*X*poly-1,3-butadiene, 29698-97-3.